J Supercond Nov Magn (2012) 25:1383–1387
DOI 10.1007/s10948-012-1524-2

ORIGINAL PAPER

Phase Separation in Electron Doped Iron-Selenide $K_{0.8}Fe_{1.6}Se_2$ Superconductor by Scanning X-ray Nano-Diffraction

A. Ricci · N. Poccia · B. Joseph · G. Campi · A. Bianconi

Published online: 28 March 2012

Abstract A new family of high temperature superconductors, the heavily electron doped iron-selenides, like $K_{0.8}Fe_{1.6}Se_2$, has been attracting high interest since they show both 30 K superconductivity, with missing hole pockets questioning the $s_\pm$ pairing model, and unusually high magnetic moments. The hot debate is between coexistence versus phase separation and on the possible divergence of surface from bulk structure. Here, we provide direct evidence for a nanoscale phase separation in a single crystal of $K_{0.8}Fe_{1.6}Se_2$, where a first magnetic phase, with superlattice modulation ($\sqrt{5}\times\sqrt{5}$), coexists with a second nonmagnetic phase, with a second superlattice modulation ($\sqrt{2}\times\sqrt{2}$), below 520 K using transmission X-ray diffraction. The mapping of the spatial distribution of the two phases is measured by scanning X-ray nanodiffraction using a 300×300 nm^2 X-ray spot. The complex spatial phase separation clarifies the coexistence of superconductivity and magnetism in the same sample.

Keywords Phase separation · High temperature superconductors · Coexistence of magnetism and superconductivity · Scanning X-ray diffraction · Nano X-ray diffraction

A. Ricci (✉) · N. Poccia · B. Joseph · A. Bianconi
Department of Physics, Sapienza University of Rome,
P. le A. Moro 2, 00185 Rome, Italy
e-mail: phd.alessandro.ricci@gmail.com

A. Bianconi
e-mail: antonio.bianconi@uniroma1.it

A. Ricci
Deutsches Elektronen-Synchrotron (DESY), Notkestraße 85,
22607 Hamburg, Germany

G. Campi
Institute of Cristallography, CNR, via Salaria Km 29.300,
Monterotondo Stazione, Roma, 00016, Italy

Superconductivity, with transition temperature, T_c, about 30 K, was reported in $K_xFe_{2-y}Se_2$ [1], which soon followed by observation of superconductivity with similar T_c in a number of similar compounds [2–6]. These systems are rather heavily electron doped compared to other Fe-based superconductors (FeSC). Moreover, they show a magnetic moment associated with the Fe-layer that is unusually high. Angle resolved photoemission (ARPES) studies [7, 8] showed that the hole pockets are completely sink under the Fermi level, due to heavy electron doping, providing a quite different Fermi surface topology from other Fe-based superconductors, where nesting between the electron and hole pockets in parent compounds has motivated the $s_\pm$ pairing model. Similar inference has been obtained from NMR [9] and specific heat [10] studies. Neutron diffraction studies [11–13] estimate the magnetic moments to be 3.3 μB per Fe site in the superconducting samples. These studies indicate that magnetism occurs in iron-deficient samples when the iron vacancies form an order $\sqrt{5}\times\sqrt{5}$ superstructure [11–14] that can be viewed as an assembly of Fe_4 square plaquettes connected at their corners. Structural models based on such vacancy ordering have been found to give excellent description of the room temperature crystal structure of these systems [15]. Several studies have identified the Fe vacancy ordering and phase separation [16, 17]. On the other hand, muon spin resonance results have been interpreted due to the coexistence of magnetism and superconductivity [18]. Some studies further suggest that superconductivity occurs only in the charge-balanced compositions with general formula $K_xFe_{2-x/2}Se_2$, and only when Fe vacancy is ordered and magnetism sets in [11–13].

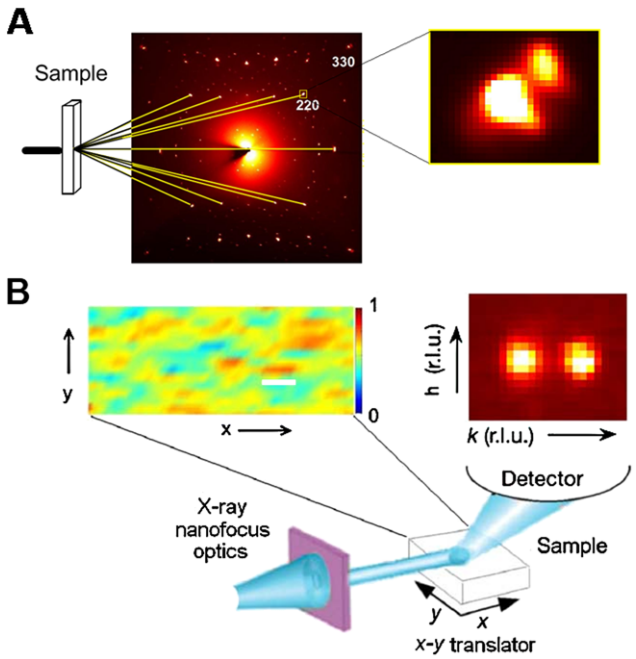

Fig. 1 (**A**) The high resolution X-ray diffraction apparatus located at the ELETTRA synchrotron radiation facility, providing stable 20 keV monochromatized X-ray beam of size approximately $200 \times 200\ \mu m^2$ by toroidal focusing optics. A charge-coupled detector (CCD) records the X-rays scattered by the sample in transmission mode. The sample temperature is controlled by a heat blower to monitor the evolution of the tetragonal crystal structure. The *upper-right panel* shows the 220 peak which splits into two spots, one with smaller lattice parameters (compressed phase) and one with similar lattice parameter (relaxed phase). (**B**) The X-ray nanofocus apparatus located at ID13 beamline at the European synchrotron radiation facility (ESRF) providing stable 14 keV monochromatized X-ray beam of size approximately $300 \times 300\ nm^2$ by KB-mirror focusing optics. *Upper-right panel* shows a CCD recording the X-rays scattered by the sample. The room temperature coexisting two phases in $K_{0.8}Fe_{1.6}Se_2$ are evidenced by the splitting of the main Brag peak reflections. The intensity of the compressed phase, $I(c)$, and of the relaxed phase, $I(r)$ is integrated over square subareas of the image recorded by the CCD detector in reciprocal-lattice (r.l.u) and then normalized to the intensity I_0 of the tail of the main crystallographic reflection at each point (x, y) of the sample reached by the translator. The nanoscale phase separation $[I(c) - I_0]/[(I(r) - I_0) + (I(c) - I_0)]$ is visualized in the color-maps. The scale bar corresponds to 5 μm

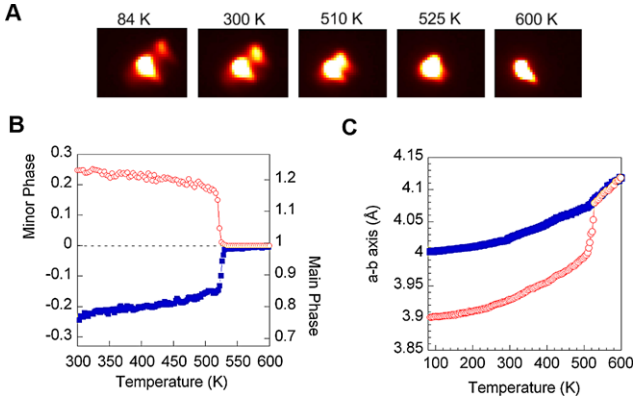

Fig. 2 (**A**) Temperature evolution of the (220) peaks at different temperatures. (**B**) The normalized peak intensity of the main and satellite peak as a function of temperature. (**C**) The lattice parameter variation with temperature

The coexistence of a high magnetic moment, with superconductivity calls for systematic probes to check whether it is a microscopic coexistence or a nanoscopic phase separation and whether there is a structural divergence between the surface and the bulk. We have undertaken comprehensive single crystal X-ray diffraction studies to address these questions. Our temperature dependent single crystal X-ray diffraction studies of superconducting $K_{0.8}Fe_{1.6}Se_2$ in transmission mode probing the bulk shows a phase separation in the system below 520 K where a first expanded phase with superlattice modulation coexists with a second collapsed phase with relative weight of 8:2 (Fig. 1 panel A). Room temperature X-ray nanodiffraction imaging of the crystal in reflection modem, shows spatial distribution of the phase separation of the compressed and expanded phases (Fig. 1 panel B). The images show the phase separation in surface regions shedding light on the origin of the coexistence of superconductivity and magnetism in these compounds.

Single crystals of nominal composition $K_{0.8}Fe_{1.6}Se_2$ showing a superconducting transition temperature $T_c = 31.8$ K [6] is used for the present study. Temperature dependent single-crystal X-ray diffraction (XRD) studies were conducted at the XRD1 beamline of the ELETTRA synchrotron radiation facility, Trieste using photons of energy 20 keV. The crystal symmetry at 600 K is found to be of tetragonal (space group I4/mmm, $ThCr_2Si_2$-type tetragonal unit-cell) with lattice parameters $a = b \approx 0.401(3)$ nm and $c \approx 1.384(3)$ nm. Differently from pnictides that show a transition of the main structure [19, 20]; below 580 K, superlattice peaks start to appear, in $K_{0.8}Fe_{1.6}Se_2$, indicating the Fe vacancy ordering. This vacancy ordered structure can be described by a $\sqrt{5} \times \sqrt{5} \times 1$ expanded unit-cell of the tetragonal phase (I4/m symmetry). Below 520 K, the system undergoes a phase separation with the appearance of a new nonmagnetic phase with slightly compressed basal lattice parameters (Fig. 2). In the meantime, a second set of superlattice reflexes with a modulation of $\sqrt{2} \times \sqrt{2} \times 1$ appeared (Fig. 3 panels A and B). We designate the phase with shorter lattice parameters as the compressed phase, while the other as relaxed phase. The X-ray diffraction in the transmission mode probes the bulk of the 200 microns thick sample and provides a probability of the compressed phase to be 25 % at room temperature (Fig. 2 panel B). This phase separation appears as a very sharp first-order transition characterized by an evident thermal hysteresis (Fig. 3 panel C). To investigate the phase separation between the compressed and expanded phases at nanoscale, the $K_{0.8}Fe_{1.6}Se_2$ single crystal, is analyzed using the scanning nanofocus diffraction facility at ID13 beamline of the European synchrotron radiation fa-

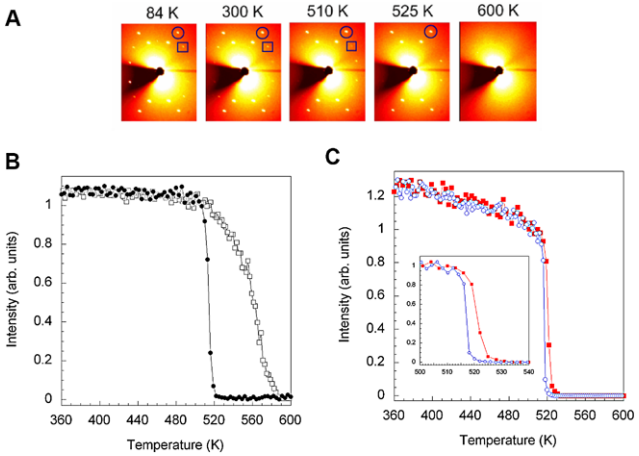

Fig. 3 (**A**) Temperature evolution of the spots (super-lattice peaks) around the beam-center at five selected temperatures. The frame marked as 525 K, show a set of super-lattice peaks ($\sqrt{5} \times \sqrt{5}$), one of which is marked with a *circle*. As one go down in temperature, a new set of super-lattice peaks ($\sqrt{2} \times \sqrt{2}$) are seen to appear. In the frame marked 510 K, a typical member in this new set of super-lattice peaks is marked by a *square*. In panel **B**, the temperature evolution of the $\sqrt{5} \times \sqrt{5}$ (*empty squares*) and $\sqrt{2} \times \sqrt{2}$ (*fill dots*) super-lattice peak intensities are shown. Panel **C** shows the sharp temperature drop of the minority phase during the heating (*red filled squares*) and it is appearing on cooling (*blue open circles*). In the *inset*, a zoom of the phase separation between a compressed (shorter a, b parameters) and expanded (longer a, b lattice parameters) phases is shown below 520 K underlining the presence of an hysteresis during the thermal cycle (Color figure online)

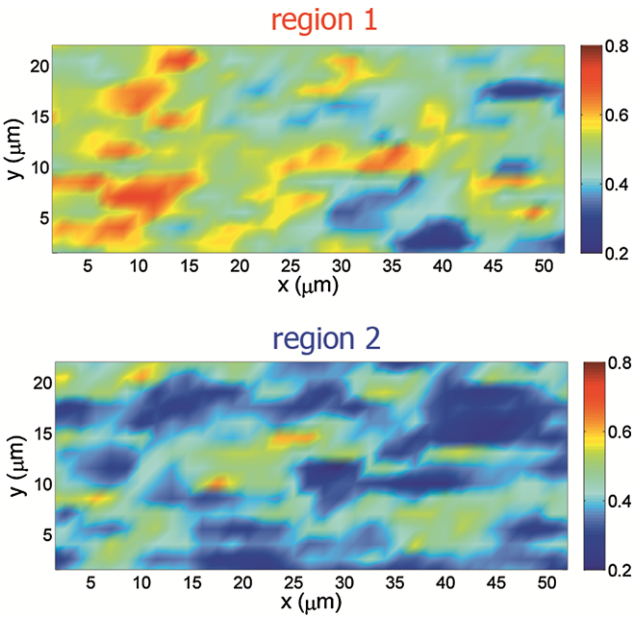

Fig. 4 The position dependence of ratio between the compressed and the expanded phase in different surface regions of size $22 \times 55\ \mu m^2$ of a $K_{0.8}Fe_{1.6}Se_2$ crystal. The crystallographic a-axis and b-axis are along the horizontal and the vertical direction. The *intense red-yellow peaks* in the two-dimensional color map represent locations of the sample with dominant compressed phase; *dark blue* indicates spots of dominant expanded phase. Two representative regions, of sample, are shown (Color figure online)

cility (ESRF), in Grenoble (Fig. 1 panel B). Measurements were done with photons of energy 14 KeV, with a 300 nm focused beam-size on the sample. The sample is fixed in a moving stage for spatial scanning to permit the maps of regions of the sample.

We first present essential results of the phase separation phenomena observed in the single crystal XRD transmission study. As mentioned earlier, the sample is in tetragonal phase at 600 K. Following the temperature dependence of the tetragonal reflections (for example, the 220 peak or the 330 peak), one can observe a splitting of the main reflections into two spots below 520 K (Fig. 2 panel A). The two new phases formed are with slightly different lattice parameters, giving a lattice strain of about 2.5 % for the one phase compared to the other. We call this strained phase as compressed phase, while the other as relaxed phase. The phase separation between phases with slightly different lattice parameter lead to the "complexity" in the system, with different co-existing local distances, with compressed and expanded phases with magnetic and superconducting electronic properties.

It is quite important to investigate the real space arrangement of the two phases in the superconducting $K_{0.8}Fe_{1.6}Se_2$. Nanofocus diffraction is a unique tool for this purpose. The experimental setup (described in Fig. 1B) is ideally suited to do the combined real and reciprocal imaging of the system. Within the same $300 \times 300\ nm^2$ crystal surface-area, illuminated by the X-ray spot, we see the coexistence of compressed and relaxed lattice domains. To have an estimate of coherence length associated with the domains of the two phases, one can resort to a peak deconvolution of the profiles. The experimental coherence length of the diffracting domains is found to be around 10 nm ($\xi^k = 1/\kappa = 9.6 \pm 2$ nm).

The spatial maps of the relaxed and compressed phases in the $K_{0.8}Fe_{1.6}Se_2$ samples have been generated by collecting the data taken at each point on the sample during the run. In particular, two regions of size $22 \times 55\ \mu m^2$ were mapped using the $K_{0.8}Fe_{1.6}Se_2$ crystal aligned in reflection mode. The intense red-yellow peaks in the two-dimensional color map in Fig. 4 (upper panel) represent locations of the sample with high strength of the three-dimensional ordering of the compressed phase, dark blue indicates spots of relaxed phase ordering. It is found that the sample contains different regions where one phase is dominant over the other. But the overall weight changes from region to region (Fig. 4 lower panel). The statistical analysis of the mapping shows fluctuations at microscale of the coexisting phases with about 20 % amplitude variation. In particular, the two maps show an over-all weight for the compressed and relaxed phase to be of 3 : 7. This value is slightly different from the bulk mea-

surements which is 2 : 8. The mapping measurements are more surface sensitive (due to the reflection geometry used). This indicates a possible different phase separation scenario at the surface and the bulk.

Present observation of an intrinsic phase separation with the coexistence of a relaxed and compressed phase to suggest the importance of inhomogeneities in the $A_xFe_{2-y}Se_2$ systems. Indeed the phase diagram of involving Fe–Se show the possibility of coexisting phases for different ratios between Fe and Se [21], consistent with extreme sensitivity of the chemical composition to the superconducting properties of FeSe [22]. The drastic increase in the T_c of the FeSe under pressure [23] further underlines the importance of the local inhomogeneities and interlayers misfit strain like in pnictides [24–26]. The coexisting chalcogen heights observed in the doped ternary chalcogenides [27–29] are found to be more pronounced in the $A_xFe_{2-y}Se_2$ systems [23–29]. The $K_xFe_{2-y}Se_2$ system with the phase separation between a magnetic phase with a superlattice and a superconducting phase with a second superlattice order recalls the case of superoxygenated La_2CuO_4 [30, 31].

Indeed the intrinsic phase separation is identified as an important feature in the cuprates both from experimental [32–36] as well as theoretical [37–39] points of view. This intrinsic phase separation has been assigned to a generic features of a multigap superconductor tuned near a Lifshitz critical point for a vanishing Fermi surface giving the shape resonance in the superconducting gaps that gives high temperature superconductivity [40, 41]. In this regime, the system is driven by doping and misfit strain [19, 24, 42] in the verge of phase separation as observed in pnictides [43] and cuprates [44]. Therefore, high T_c superconducting emerges in a metallic phase near a quantum critical regime in a complex granular material.

Acknowledgements We thank M. Colapietro, the Elettra XRD beamline staff in Trieste and the ESRF XRD 13 beamline staff in Grenoble for experimental help. This experimental work has been carried out with the financial support of Sapienza University of Rome, research project "Stripes and High-T_c Superconductivity."

References

1. Guo, J., et al.: Phys. Rev. B **82**, 180520 (2010). doi:10.1103/PhysRevB.82.180520
2. Krzton-Maziopa, A., et al.: J. Phys., Condens. Matter **23**, 052203 (2011). doi:10.1088/0953-8984/23/5/052203
3. Wang, A.F., et al.: Phys. Rev. B **83**, 060512 (2011). doi:10.1103/PhysRevB.83.060512
4. Wang, H.-D., et al.: Europhys. Lett. **93**, 47004 (2011). doi:10.1209/0295-5075/93/47004
5. Fang, M.-H., et al.: Europhys. Lett. **94**, 27009 (2011). doi:10.1209/0295-5075/94/27009
6. Mizuguchi, Y., et al.: Appl. Phys. Lett. **98**, 042511 (2011). doi:10.1063/1.3549702
7. Zhao, L., et al.: Phys. Rev. B **83**, 140508 (2011). doi:10.1103/PhysRevB.83.140508
8. Mou, D., et al.: Phys. Rev. Lett. **106**, 107001 (2011). doi:10.1103/PhysRevLett.106.107001
9. Ma, L., He, J.B., Wang, D.M., Chen, G.F., Yu, W.: Preprint. arXiv:1101.3687v1 (2011)
10. Zeng, B., et al.: Phys. Rev. B **83**, 144511 (2011). doi:10.1103/PhysRevB.83.144511
11. Bao, W., et al.: Preprint. arXiv:1102.0830v1 (2011)
12. Bao, W., et al.: Preprint. arXiv:1102.3674v1 (2011)
13. Zavalij, P., et al.: Phys. Rev. B **83**, 132509 (2011). doi:10.1103/PhysRevB.83.132509
14. Ye, F., et al.: Phys. Rev. Lett. **107**, 137003 (2011). doi:10.1103/PhysRevLett.107.137003
15. Pomjakushin V.Yu., et al.: Phys. Rev. B **83**, 144410 (2011). doi:10.1103/PhysRevB.83.144410
16. Ricci, A., et al.: Supercond. Sci. Technol. **24**, 082002 (2011)
17. Ricci, A., et al.: Phys. Rev. B **84**, 060511 (2011). doi:10.1103/PhysRevB.84.060511
18. Shermadini, Z., et al.: Phys. Rev. Lett. **106**, 117602 (2011). doi:10.1103/PhysRevLett.106.117602
19. Ricci, A., et al.: Phys. Rev. B **82**, 144507 (2010). doi:10.1103/PhysRevB.82.144507
20. Ricci, A., Fratini, M., Bianconi, A.: J. Supercond. Nov. Magn. **22**, 305–308 (2009). doi:10.1007/s10948-008-0434-9
21. Predel, B.: Fe–Se (Iron–Selenium). In: Madelung, O. (ed.) SpringerMaterials—The Landolt–Börnstein Database. doi:10.1007/10474837_1339
22. McQueen, T.M., et al.: Phys. Rev. B **79**, 014522 (2009). doi:10.1103/PhysRevB.79.014522
23. Medvedev, S., et al.: Nat. Mater. **8**, 630–633 (2009). doi:10.1038/nmat2491
24. Ricci, A., Poccia, N., Ciasca, G., Fratini, M., Bianconi, A.: J. Supercond. Nov. Magn. **22**, 589–593 (2009). doi:10.1007/s10948-009-0473-x
25. Xu, W., et al..: Europhys. Lett. **90**, 57001 (2010). doi:10.1209/0295-5075/90/57001
26. Ricci, A., et al.: Supercond. Sci. Technol. **23**, 052003 (2010). doi:10.1088/0953-2048/23/5/052003
27. Joseph, B., et al.: Phys. Rev. B **82**, 020502 (2010). doi:10.1103/PhysRevB.82.020502
28. Iadecola, A., et al.: Europhys. Lett. **90**, 67008 (2010). doi:10.1209/0295-5075/90/67008
29. Joseph, B., et al.: J. Phys., Condens. Matter **22**, 485702 (2010). doi:10.1088/0953-8984/22/48/485702
30. Fratini, M., et al..: Nature **466**, 841–844 (2010). doi:10.1038/nature09260
31. Poccia, N., et al.: Nat. Mater. **10**, 733–736 (2011). doi:10.1038/nmat3088
32. Jorgensen, J.D., et al.: Phys. Rev. B **38**, 11337–11345 (1988). doi:10.1103/PhysRevB.38.11337
33. Mohottala, H.E., et al.: Nat. Mater. **5**, 377–382 (2006). doi:10.1038/nmat1633
34. Poccia, N., et al.: Phys. Rev. B **84**, 100504 (2011). doi:10.1103/PhysRevB.84.100504
35. Beyers, R., et al.: Nature **340**, 619–621 (1989). doi:10.1038/340619a0
36. Tranquada, J.M., et al.: Phys. Rev. Lett. **78**, 338–341 (1997). doi:10.1103/PhysRevLett.78.338
37. Dagotto, E., et al.: Phys. Rev. B **49**, 3548–3565 (1994). doi:10.1103/PhysRevB.49.3548
38. De Mello, E.V.L., Kasal, R.B., Passos, C.A.C.: J. Phys., Condens. Matter **21**, 235701 (2009). doi:10.1088/0953-8984/21/23/235701
39. Kugel, K.I., et al.: Phys. Rev. B **78**, 165124 (2008). doi:10.1103/PhysRevB.78.165124

40. Innocenti, D., et al.: Supercond. Sci. Technol. **24**, 015012 (2011). doi:10.1088/0953-2048/24/1/015012
41. Innocenti, D., Poccia, N., Ricci, A., Valletta, A., Caprara, S., Perali, A., Bianconi, A.: Phys. Rev. B **82**, 184528 (2010). doi:10.1103/PhysRevB.82.184528
42. Fratini, M., Caivano, R., Puri, A., Ricci, A., Ren, Z.-A., Dong, X.-L., Yang, J., Lu, W., Zhao, Z.-X., Barba, L., Arrighetti, G., Polentarutti, M., Bianconi, A.: Supercond. Sci. Technol. **21**, 092002 (2008). doi:10.1088/0953-2048/21/9/092002
43. Caivano, R., et al.: Supercond. Sci. Technol. **22**, 014004 (2009). doi:10.1088/0953-2048/22/1/014004
44. Bianconi, A.: Int. J. Mod. Phys. B **14**, 3289–3297 (2000). doi:10.1142/S0217979200003769